International Journal of Hydrogen Energy 82 (2024) 374–383

Contents lists available at ScienceDirect

International Journal of Hydrogen Energy

journal homepage: www.elsevier.com/locate/he

Remaining useful life prognostic-based energy management strategy for multi-fuel cell stack systems in automotive applications

W. René Bankati [a,b,*], Loïc Boulon [a], Samir Jemei [b]

[a] Hydrogen Research Institute, Université Du Québec à Trois-Rivières, Trois-Rivières, Qc, Canada
[b] Université de Franche-Comté, CNRS, Institut FEMTO-ST, FCLAB, F-90000, Belfort, France

ARTICLE INFO

Handling Editor: Ramazan Solmaz

Keywords:
Multi-fuel cell stack systems
Remaining useful life
Prognostic
Energy management strategy
Fuel cell hybrid electric vehicle

ABSTRACT

To achieve the 8000-h proton exchange membrane fuel cell stack (PEM FCS) life target set by the U.S DoE and promote fuel cell hybrid electric vehicles (FCHEVs) massive introduction in the automotive market, using multi-fuel cell stack (MFCS) systems instead of single-fuel cell stack systems seems to be an interesting solution that deserves to be explored. MFCS systems' concept combines several small FCSs modules instead of using a single high-powered FCS module. The modularity in such systems can be exploited through energy management to improve their durability and extend their good energy-efficiency power range. However, FCSs' multiplicity makes it challenging to implement effective energy management strategies (EMSs). This paper proposes a remaining useful life (RUL) prognostic-based EMS to extend MFCS systems' lifetime while keeping their hydrogen consumption reasonable. For this purpose, a prognostic algorithm is developed to predict PEM FCSs' RUL in real-world automotive application scenarios. Then a rule-based EMS allocates the demand between stacks using prognostic results. The proposed strategy's performance is evaluated on a hybrid MFCS/battery system using Matlab/Simulink's environment. Simulation results show that implementing the proposed strategy instead of conventional EMSs can extend MFCS systems' lifetime by at least a factor of 2.35 while keeping their hydrogen consumption reasonable.

1. Introduction

Using hydrogen through PEM FCSs as vehicle power sources is a promising solution to decarbonize transportation [1,2]. However, their low durability is a significant issue that hinders FCHEVs promotion [3,4]. According to the U.S. Department of Energy (U.S. DoE), PEM FCSs' lifetime, currently about 5000 h, must be increased to at least 8000 h to promote FCHEVs massive introduction in the automotive market [5,6]. From this point of view, adopting the MFCS systems concept appears to be an attractive solution. It should be noted that MFCS systems have already been used in marine transport and aeronautics with the U212A-class Todaro [7] and the four-seat H4Y aircraft [8] for example. In fact, due to their high modularity, MFCS systems could offer more degrees of freedom to EMSs to make energy management decisions that can extend their lifetime, reduce their hydrogen consumption, and improve their reliability [9–11]. MFCS systems concept advantages could even go beyond these three criteria, by addressing the question of cost from economies of scale's angle.

The proof-of-concept of MFCS systems concerning the four criteria (durability, energy efficiency, reliability, and cost) mentioned before involves the implementation of efficient EMSs. Consequently, energy management is the most addressed issue in the literature regarding MFCS systems. MFCS systems' EMSs that are proposed in the literature can be divided into two categories: rule-based EMSs and optimization-based EMSs. An optimization-based EMS and a rule-based EMS are respectively proposed for MFCS systems in Refs. [12,13] to improve the conventional Daisy-Chain strategy. Both strategies were found capable of reducing MFCS systems' hydrogen consumption respectively by 9.42 % and 7% compared to the basic Daisy-Chain EMS. However, the MFCS systems' lifetime has not been evaluated, so it cannot be concluded whether these strategies improve MFCS systems' durability or not. Several other Rule-based EMSs [14,15] and optimization-based EMSs [16–20] are designed to reduce MFCS systems' hydrogen consumption while durability consideration is suggested as a potential future work. Even in research papers where FCSs' degradation is considered in MFCS systems energy management such as [21–26], the lifetime improvement is not quantified.

The review of MFCS systems' EMSs highlights the ability of most

* Corresponding author. Hydrogen Research Institute, Université du Québec à Trois-Rivières, Trois-Rivières, Qc, Canada.
E-mail address: rene.bankati@uqtr.ca (W.R. Bankati).

https://doi.org/10.1016/j.ijhydene.2024.07.448
Received 24 May 2024; Received in revised form 23 July 2024; Accepted 30 July 2024

strategies to optimize MFCS systems' hydrogen consumption. Furthermore, it shows that the literature lacks EMSs that are likely to enhance MFCS systems' lifetime. Therefore, this paper aims to contribute to addressing this issue by proposing a health-conscious EMS for improving MFCS systems' durability.

FCS and MFCS systems' health-conscious EMSs can be divided into two categories: diagnostic-based EMSs and prognostic-based EMSs.

Prognostic-based EMSs are part of the Prognostic and Health Management (PHM) discipline [27], which consists of 7 modules: data acquisition, data processing, condition assessment, diagnostics, prognostics, decision-making, and human-machine interface. A detailed description of each one of these modules can be found in Ref. [28]. Prognostic-based EMSs are complementary to diagnostic-based EMSs [29–32], as they have more available information like FCSs' remaining useful life (RUL) for decision-making even if no operating anomalies are detected. This allows them to adjust energy management rules before faults occur, making them more efficient than diagnostic-based EMSs. FCSs' RULs are predicted by prognostic algorithms, which can be implemented using different approaches: the model-based approach [33,34], the data-driven approach [35–39], the hybrid approach [40, 41], or the experience-based approach [42].

It should be acknowledged that a great deal of progress has already been made in terms of prognostic methods to help energy management decision-making for FCS or MFCS systems. Two RUL prognostic-based EMSs were proposed in Refs. [6,43] for a range-extender FCHEV. In Ref. [44], an end-of-life prognostic-based EMS was applied to an MFCS system made up of three PEM FCSs. By solving a multi-objective optimization problem, this strategy extended the MFCS system's lifetime by around 25% compared to the Daisy-Chain strategy, without increasing its hydrogen consumption.

Several other researchers in Refs. [45–47], found that RULs prognostic-based EMSs have the potential to significantly enhance FCS or MFCS systems' durability. However, despite the abundance of prognostic methods in the literature, the number of proposed prognostic-based EMSs is very limited. This discrepancy can be attributed to the fact that integrating FCS prognostic methods into energy management requires additional research, as these two fields of expertise are distinct. Prognostic involves signal processing and data analysis skills, while energy management demands expertise in systems engineering. This paper proposes an EMS for MFCS systems based on RUL prognostic, combining the strengths of these two fields of expertise to enhance such systems' durability.

The present paper will be structured as follows: a PEM FCS aging model will be established in section 2 based on various researchers' FCS modeling works. In Section 3, an ANN-based FCS prognostic algorithm will be proposed for real-world use in automotive applications to investigate the prognostic-based energy management concept under a real vehicle use scenario. An MFCS system RUL prognostic-based EMS will be suggested in section 4. The strategy will be applied to a hybrid MFCS system/battery in section 5 and the simulation results will be presented and compared to two conventional EMSs' results. In section 6, the proposed EMS will be compared with a state of health (SOH) estimation-based EMS, which appears as the reference EMS in this study regarding the applied energy management principle.

2. PEM FCS model with aging consideration

In this paper, the PEM FCS model is established based on previous modeling works that have been suggested in the literature for energy management purposes.

2.1. PEM FCS static and dynamic models

- PEM FCS static model:

The static model is based on the polarization equation of an N-cell PEM FCS.

$$V(i_{FC}, T_{FCS}, P_{O_2}, P_{H_2}) = N[E_{rev}(T_{FC}, P_{O_2}, P_{H_2}) - \Delta E_{act}(i_{FC}, T_{FC}) - \Delta E_{conc}(i_{FC}, T_{FC}) - \Delta E_{ohm}(i_{FC})] \quad (1)$$

$$E_{rev}(T_{FC}, P_{O_2}, P_{H_2}) = \frac{T_{FC}.\Delta S - \Delta H}{2F} + \frac{R.T_{FC}}{2F} \ln\left(\frac{P_{H_2}.P_{O_2}^{\frac{1}{2}}}{P_{O_2}^{\frac{3}{2}}}\right) \quad (2)$$

$$\Delta E_{act}(i_{FC}, T_{FC}) = A.T_{FC} \ln\left(\frac{i_{FC} + i_n}{i_0}\right) \quad (3)$$

$$\Delta E_{conc}(i_{FC}, T_{FC}) = -B.T_{FC} \ln\left(1 - \frac{i_{FC}}{i_l}\right) \quad (4)$$

$$\Delta E_{ohm}(i_{FC}) = R_{FC}.i_{FC} \quad (5)$$

Where i_{FC} is the FCS current density; V represents the stationary part of the FCS output voltage; E_{rev} is the reversible Nernst potential; ΔE_{act}, ΔE_{conc}, and ΔE_{ohm} symbolize activation losses, concentration losses and ohmic losses respectively. T_{FC} is the operating temperature of the FCS; P_{O_2} and P_{H_2} are oxygen partial pressure and hydrogen partial pressure respectively. ΔS denotes the entropy variation while ΔH stands for the energy released by the reaction taking place in the FCS. R and F are respectively the gas constant and the Faraday constant.

- PEM FCS dynamic model:

In PEM FCS, during power variations, the temperature transient is the slowest physical phenomenon to occur before stabilization in the steady state. As a result, this study will only focus on thermal dynamics modeling.

The slow dynamics effects of thermal phenomena on the FCS voltage can be seen as an additional voltage $N.V_{dyn}(t)$ which is characterized by a transient and steady state [48]. The FCS output voltage $V_{FCS}(t)$ can then be written as follows:

$$V_{FCS}(t) = V + N.V_{dyn}(t) \quad (6)$$

Where:

$$\frac{i_{FC}(t)}{\tau_{dyn}} = \frac{dV_{dyn}(t)}{dt} + \frac{V_{dyn}(t)}{\tau_{dyn}} \quad (7)$$

To approximate a real PEM FCS system dynamic, the time constant τ_{dyn} will be set so that the steady state of the output voltage should be established after 300 s. Thus, to preserve FCSs' SOH in transport applications, it is important to filter the mission profile's dynamics. In this case, using a power source such as a battery to hybridize the FCS or the MFCS system is necessary.

- Battery and DC-DC converter models for PEM FCS systems

An empirical battery model (Fig. 1) that includes an open-circuit voltage source V_0 connected in series with a resistance $R_{s_{bat}}$, and a parallel circuit consisting of a resistance $R_{c_{bat}}$, and a capacitance $C_{c_{bat}}$ is adopted in this paper. The values of these parameters can be estimated experimentally on the real battery that will be chosen after system sizing.

From the equivalent electrical circuit illustrated in Fig. 1, the current of the battery, i_{bat}, can be expressed by the equation (8).

$$i_{bat} = \frac{V_0 - R_{s_{bat}} i_{bat} - V_{bat}}{R_{c_{bat}}} + C_{c_{bat}} \frac{d}{dt}\left(V_0 - R_{s_{bat}} i_{bat} - V_{bat}\right) \quad (8)$$

Equation (9) can be used to calculate the instantaneous state of charge $SOC_{bat}(t)$ of the battery given its initial state of charge $SOC_{bat_{init}}$, capacity Q_{bat}, and current i_{bat}. The initial state of charge $SOC_{bat_{init}}$ will be set arbitrarily before starting each simulation in this study.

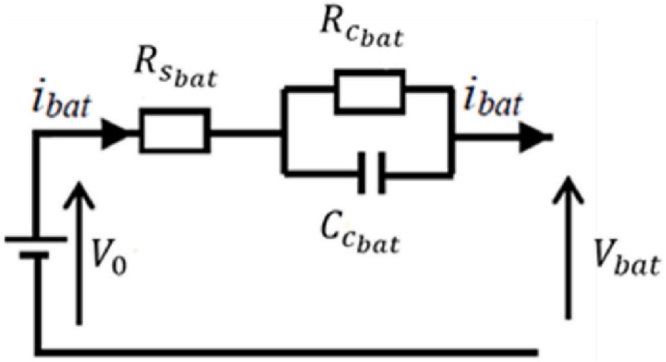

Fig. 1. Battery model.

$$SOC_{bat}(t) = SOC_{bat_{init}} - \frac{100}{3600Q_{bat}} \int i_{bat} dt \tag{9}$$

As the study focuses on FCS aging, battery aging is neglected due to the longer lifetime of batteries compared to FCS (over 45,000 h vs. approx. 5000 h). Therefore, battery degradation will not be modelled. However, a boost DC-DC converter model is necessary to increase FCSs' output voltage before connecting them to the DC bus and to regulate their current.

If L_{boost} and V_{boost} represent the smoothing inductor and the converter output voltage, respectively, the current $i_{L_{boost}}$ flowing through the inductor can be obtained by the equation (10), neglecting the effect of the inductor's internal resistance.

$$i_{L_{boost}} = \frac{1}{L_{boost}} \int (V_{bat} - V_{boost}) dt \tag{10}$$

Where the converter's output voltage V_{boost} and output current I_{boost} depend on its modulation ratio α_{boost} and efficiency η_{boost} (equation (11)).

$$\begin{cases} V_{boost} = \alpha_{boost} V_{bat} \\ i_{boost} = \alpha_{boost} I_{PAC} \eta_{boost} \end{cases} \tag{11}$$

2.2. PEM FCS cycling aging model

PEM FCS degradation can be caused by several factors such as the frequency or the number of start-stop cycles $N_{switch}(t)$, operating power point $P_{FCS}(t)$, and mission profile dynamics $\frac{dP(t)}{dt}$ [49]. Developing and assessing a degradation model $\Delta_{FCS}(t)$ that considers these main FCS's aging factors could be a good approach to simulate FCS aging due to cycling. Where appropriate, the obtained degradation term can be applied to the FCS's maximum performance to reproduce its power loss as it degrades. Fig. 2 illustrates this process.

In this study, the FCS degradation model is inspired by the one suggested in Ref. [50], which considers the impact of both the number of start-stop cycles and the operating point. The profile dynamics degradation impact on the FCS's SOH is not modelled in this study as the MFCS system will be hybridized by a battery to filter the profile dynamics.

The degradation term will be applied to the electrochemical active surface area $ECSA_{FCS}(t)$ to update the FCS's maximum performance. In fact, the decrease in ECSA often represents the direct cause of FCS power loss as it ages. As shown by equation (12), the ultimate ECSA $ECSA_{FCS\_deg}(t)$ can be expressed as a function of the degradation term $\Delta_{FCS}(t)$ and the $ECSA_{FCS}(t)$, which only changes due to normal degradation of the catalyst layer.

$$ECSA_{FCS\_deg}(t) = [1 - \Delta_{FCS}(t)].ECSA_{FCS}(t) \tag{12}$$

$$\Delta_{FCS}(t) = \int_0^t \delta(t) dt + N_{switch}(t).\Delta_{switch} \tag{13}$$

$$\delta(t) = \frac{\delta_0}{3600}\left[1 + \frac{\alpha}{P_{FCS_{nom}}{}^2}(P_{FCS}(t) - P_{FCS_{nom}})^2\right] \tag{14}$$

Where:

$$P_{FCS_{nom}} = \begin{cases} 25\%P_{FCS_{max}} & si\ P_{FCS}(t) < 25\%P_{FCS_{max}} \\ P_{FCS}(t) & si\ 25\%P_{FCS_{max}} \le P_{FCS}(t) \le 95\%P_{FCS_{max}} \\ 95\%P_{FCS_{max}} & si\ P_{FCS}(t) > 95\%P_{FCS_{max}} \end{cases} \tag{15}$$

$\delta(t)$ denotes the degradation rate related to the FCS operating point. In this study, $[25\%P_{FCS_{max}}; 95\%P_{FCS_{max}}]$ will be considered as FCSs' safe power range [51,52], i.e. the power range corresponding to the lowest degradation rate ($\delta(t) = \frac{\delta_0}{3600}$), as it delimits approximately the ohmic losses region. In fact, using FCS in the ohmic losses region can prevent it from the activation and concentration phenomena that accelerate aging. If the FCS operates at low current densities, which means the operating point is close to OCV, it may experience activation losses. The degradation rate $\delta(t)$ is determined by the relative difference between the FCS output power and the nearest safe power which is $25\%P_{FCS_{max}}$. Similarly, if the FCS delivers power very close to its maximum power $P_{FCS_{max}}$, it is subject to concentration losses. The degradation $\delta(t)$ rate is determined by the relative difference between the FCS output power and the nearest safe power which is $95\%P_{FCS_{max}}$ in this case.

Δ_{switch} is the degradation caused by a single start-stop cycle, while

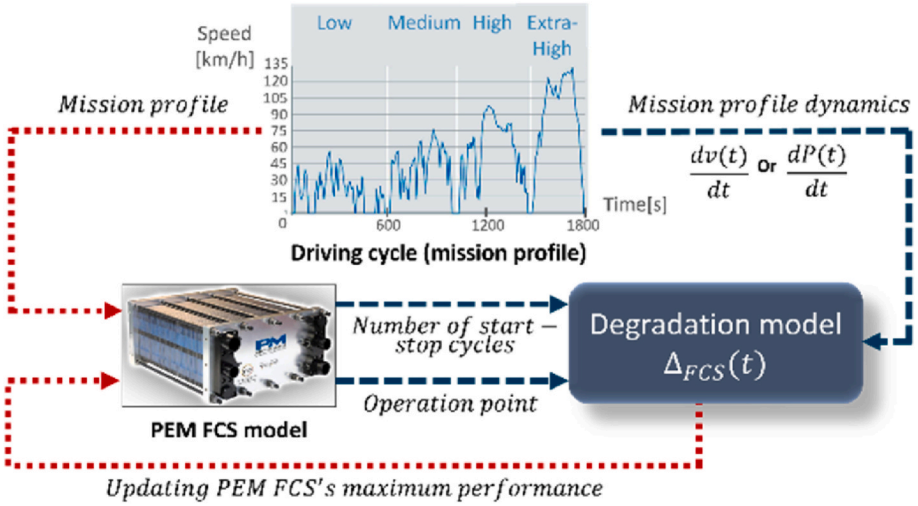

Fig. 2. Cycling aging integration approach into PEM FCS model.

$N_{switch}(t)$ denotes the total number of start-stop cycles that the FCS has undergone since its first use. δ_0, α, and Δ_{switch} are empirical parameters. Polarization tests will be conducted during simulations every 200 h to assess FCSs' SOH considering their slow aging process. The maximum power $P_{FCS_{max}}$ will be considered as FCSs' health indicator in this paper, since the output voltage may not be reliable in dynamic current profile applications. Furthermore, $P_{FCS_{max}}$ estimation will help determining FCSs' safe power range, which is defined regarding their maximum power (equation (15)).

By estimating the maximum power regularly, its future temporal evolution can be predicted over a specified prediction horizon for FCSs' RUL estimation.

3. ANN-based prognostic algorithm for FCSs real-world use in automotive applications

As shown in Fig. 3, the data-driven approach makes a good trade-off between the precision, complexity, and applicability. Therefore, it will be adopted for FCSs' SOH prediction and RUL estimation in this study.

3.1. Backpropagation neural network-based prognostic algorithm for FCSs real world use in automotive applications

As shown in Fig. 4, the basic architecture of a backpropagation neural network (BPNN), typically comprises an input layer, one or more hidden layers, and an output layer.

BPNN has been used in previous studies, such as in Refs. [35,53], to develop prognostic algorithms for FCS RUL estimation. However, like most data-driven RUL prognostic methods, these algorithms are implemented and tested with the assumption that, the future operating conditions $\{X_2, X_3, \ldots, X_n\}$ of FCSs such as current, relative humidity, gas pressure, temperature, etc., relative to the prediction horizon (the time vector X_1) would be known in the prediction phase. This assumption may not be acceptable in automotive applications, especially as RUL prognostic requires a prediction over a very long horizon (~ several hundred or even several thousand hours).

To address this issue, a BPNN-based RUL prognostic algorithm for FCSs in real-world scenarios is developed in this study so that only the time vector should be required as input to predict over a given horizon in the prediction phase.

The learning phase involves two steps that enable the network to characterize the FCS degradation trend: a forward propagation phase and the error backpropagation phase. A detailed description of each phase can be found in Refs. [35,53] with the related equations.

4. MFCS system RUL prognostic-based energy management strategy

A rule-based approach is adopted for FCSs' RULs prognostics integration in MFCS systems energy management in this paper. The proposed EMS will be referred to as the RUL prognostic-based adaptive Daisy-Chain strategy.

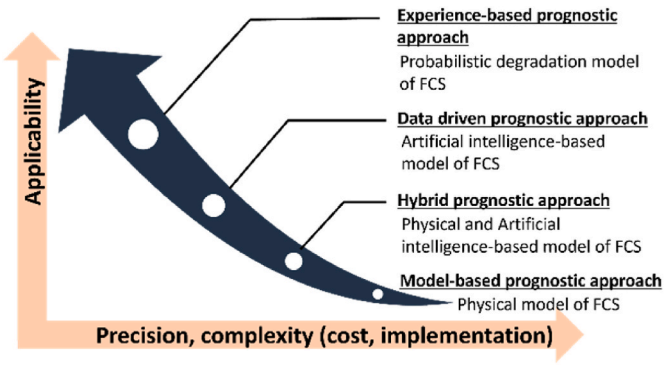

Fig. 3. Prognostic approaches classification according to precision, complexity, and applicability criteria.

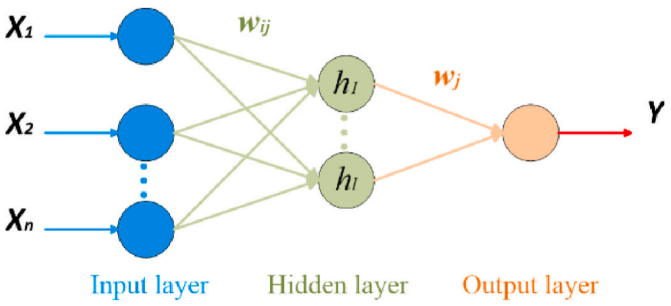

Fig. 4. Basic architecture of the BPNN.

4.1. Daisy-Chain principle

The Daisy-Chain principle is a basic strategy of operating an MFCS system. It involves activating the FCS one by one until all the required power is supplied, or until all the FCS are used.

This principle takes advantage of MFCS systems' modularity, as it always activates the minimum number of FCS needed to meet a power demand. However, the non-delimitation of FCSs' operating power ranges accelerates their degradation. Additionally, since FCSs are always used in the same order, some FCSs may age faster than others due to overuse.

In this paper, the RUL prognostic-based adaptive Daisy-Chain strategy will ensure that all FCSs in the MFCS system reach their end-of-life (EoL) at approximately the same time to prevent the MFCS system from too early degraded mode operation. Operating in degraded mode signifies that the MFCS system is reaching its EoL, as it will eventually be unable to meet the load requirements.

4.2. RUL prognostic-based adaptive Daisy-Chain energy management strategy

For the FCSs to reach their EoL at almost the same time, their degradation levels must be balanced throughout their operating time. To do so, first, FCSs scheduling is updated in descending order of RULs each time the RULs predictions are made, as shown in Fig. 5. RUL predictions will be performed every 1000 h in this paper to allow the prognostic model to learn FCSs' degradation trend properly, considering that FCSs' aging is a relatively slow process.

The obtained scheduling is updated a second time based on FCSs' previous operating modes to assign to the most degraded FCS the rank that would make it possible to slow down its aging. It should be noted that the first FCS in the queue may not always age faster than the other FCSs, under the Daisy-Chain principle, as the power requested from the MFCS system would be greater than 0 W most of the time due to the mission profile dynamics filtering. Actually, FCSs' start-stop cycles could be reduced by assigning each FCS the top position in the scheduling from time to time. Therefore, after the first scheduling in descending order of RULs, the following adjustments should be made to obtain the final scheduling of FCSs.

- The FCS that has the biggest RUL, which is the first FCS in the queue, must be moved to the rank previously occupied by the FCS that has the lowest RUL.
- The FCS that has the lowest RUL must then move to the front of the queue to slow down its aging process.
- If the FCS with the lowest RUL was the first FCS in the previous final scheduling, all FCSs must be used in the same order as before. In fact, since the first rank corresponds to the slowest degradation rate, if the

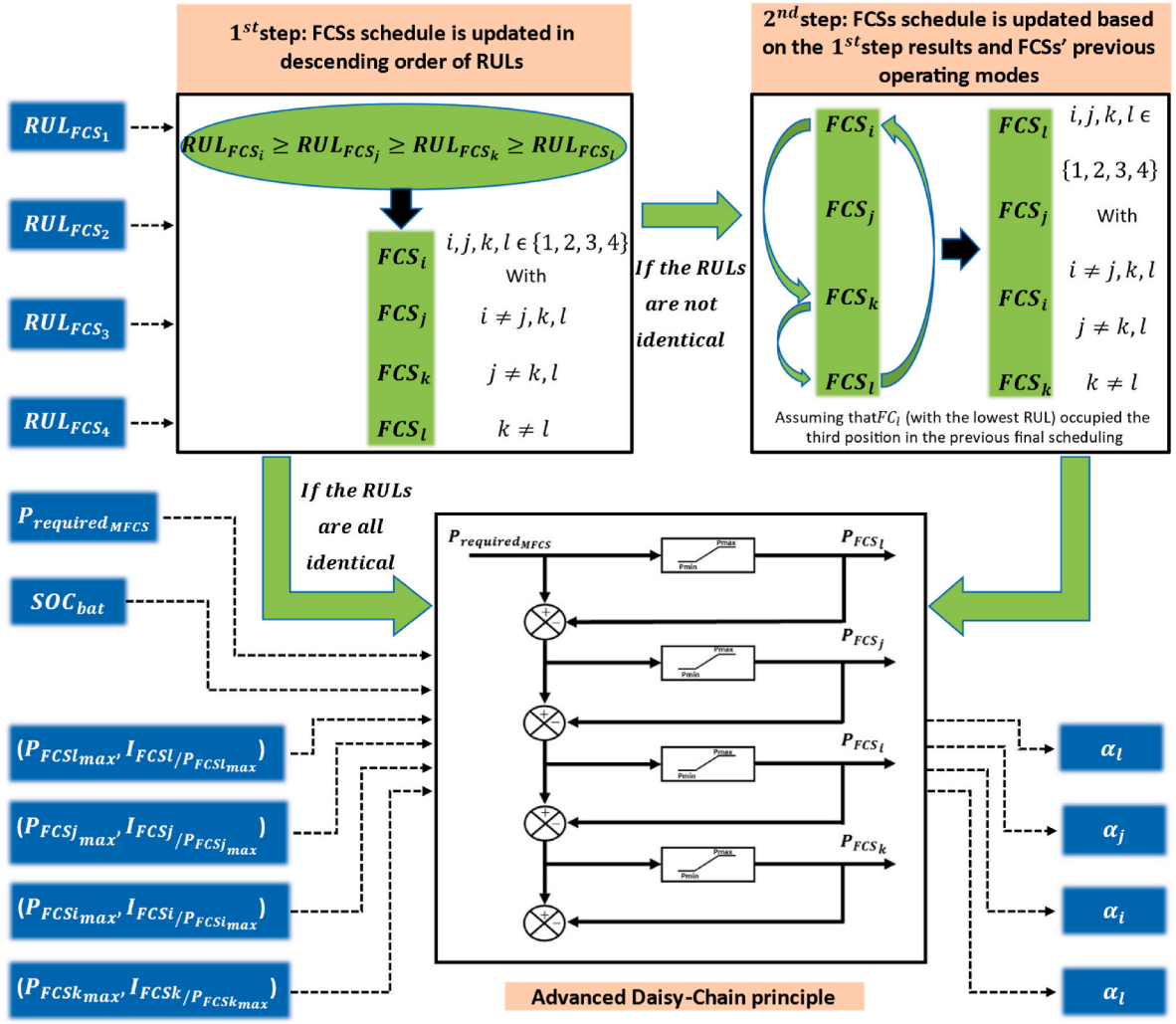

Fig. 5. Operating principle of the RUL prognostic-based adaptive Daisy-Chain EMS considering four FCSs and assuming that the FCS with the lowest RUL occupied the third place in the previous final scheduling.

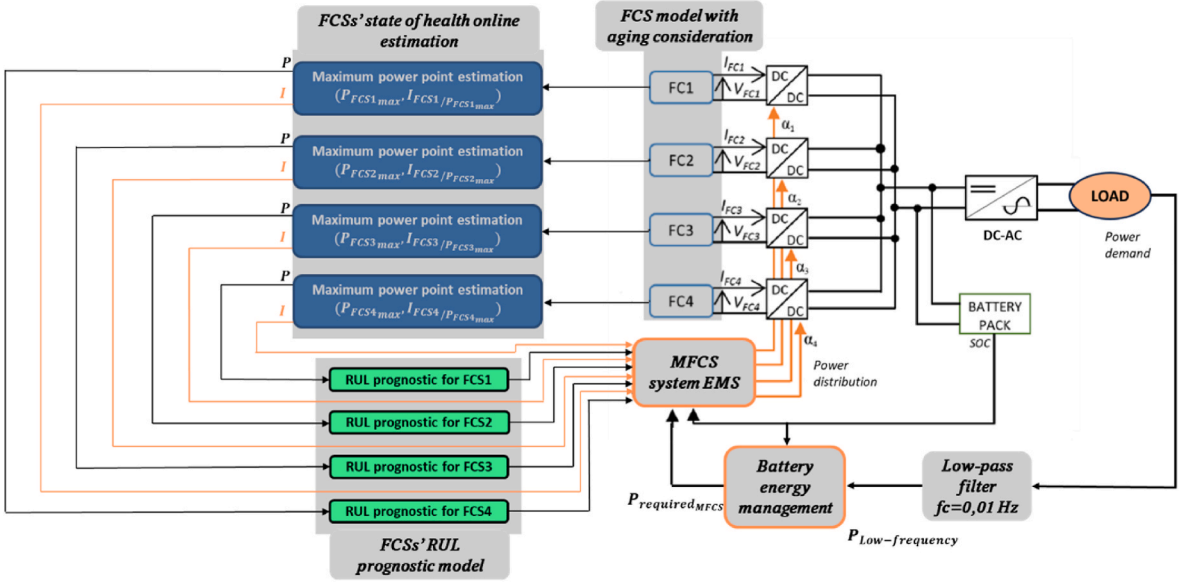

Fig. 6. Synoptic diagram of MFCS systems' RUL prognostic-based energy management concept.

FCS with the lowest RUL occupied the first rank previously, that means that it is still more degraded than all other FCSs.

Fig. 5 illustrates the RUL prognostic-based adaptive Daisy-Chain EMS considering four FCSs and assuming that the FCS with the lowest RUL occupied the third position in the previous final scheduling. This figure depicts the MFCS system EMS block that appears in Fig. 6.

In the next section, the performance of the proposed EMS will be evaluated on a hybrid MFCS/battery system using the WLTP class 3 driving cycle and compared to two conventional EMSs'.

5. Simulation results

5.1. Hybrid MFCS/battery system design choices

Several design choices and assumptions have been made regarding the hybrid MFCS/battery system to simplify the study [54,55].

- Parallel fluidic and electrical architectures are adopted to make the MFCS system as modular as possible, to offer the maximum degrees of freedom to the EMS for decision-making.
- The battery is connected directly to the DC bus, without using a converter. This topology reduces the volume, weight, and cost of the system. It also simplifies energy management between the battery and the MFCS system.
- The battery SOC variation range is restricted to 20% to limit DC bus voltage fluctuations, as this voltage would be imposed by the battery under the adopted topology.
- The DC bus voltage is assumed to be 72 V to match the DC bus voltage on the test bench.
- The MFCS system consists of 500 W-FCS systems, to ensure that power levels during simulations match those on the test bench. Therefore, the power profile obtained by applying the Newton's second law of motion to a regular-sized car is rescaled while keeping the dynamics.
- The hybrid MFCS/battery system sizing is done regarding the power profile under the WLTP class 3 standard, as this cycle reproduces real driving conditions. Thereby, it is assumed that the hydrogen tank always contains enough hydrogen, and that the vehicle's range is not limited.
- The hybrid MFCS/battery system sizing is done based on mission profile frequency decomposition technique. A low-pass filter with a cut-off frequency of 10 mHz is used for this purpose. As a result, it was found that at least four 500 W-FCS and a 20 Ah-battery would be necessary to respond to the WLTP rescaled profile.

The synoptic diagram of MFCS systems' RUL prognostic-based energy management concept is presented in Fig. 6. The battery energy management module makes sure that the battery's SOC remains between 40% and 60% to limit fluctuations in the DC bus voltage. When the battery gets discharged, it needs to be recharged with an additional current of 4 A from the MFCS system. The charging current is based on the recommended charging current range which is 10%–20% of the battery's nominal capacity. The modes that define the charged and discharged states of the battery are summarized by the hysteresis cycle depicted in Fig. 7.

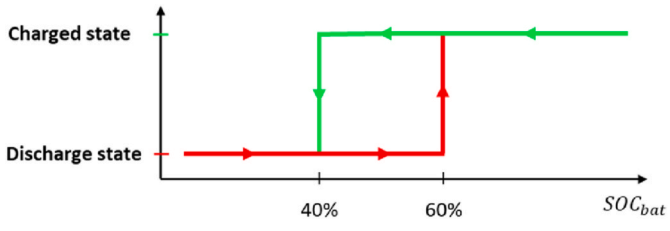

Fig. 7. Battery's charged and discharged states defined by a hysteresis cycle.

5.2. Hybrid MFCS/battery system simulation results under the proposed EMS

The distribution of $P_{required_{MFCS}}$ between the four FCS systems by the RUL prognostic-based adaptive Daisy-Chain EMS proposed in this paper is shown in Fig. 8. It should be noted that, from 0 h to 1000 h, the FCSs were used in the same way under the equidistributional EMS, while the first training data of the prognostic algorithm were collected to perform the RUL prediction for the first time at $t = 1,000\,h$. From 1000 h to 2000 h, the FCSs were operated in the initial order, i.e., FCS N°1, FCS N°2, FCS N°3, FCS N°4, as they had the same RUL at $t = 1,000\,h$, which is 37,000 h (Fig. 9). As shown in Fig. 10, using the FCSs in this order resulted in more degradation on FCS N°4 compared to FCS N°2, whose degradation was also important than that of FCS N°3. The FCS N°1, which was the first FCS in the queue form 1000 h to 2000 h, had the biggest RUL at $t = 2,000\,h$ (Fig. 9), since it was never shut down in that time range, making it the FCS that experienced the least start-stop cycles. Consequently, at $t = 2,000\,h$, FCSs scheduling in descending order of RULs was FCS N°1, FCS N°3, FCS N°2, and FCS N°4. The second scheduling had to be performed, as the RULs were not equal. The FCS N°4 with the lowest RUL had to be moved to the first position, while the FCS N°1 with the highest RUL had to be moved to the position that was previously occupied by the FCS N°1 from 1000 h to 2000 h, meaning the fourth position. Thus, the expected operation order of FCSs from 2000 h to 3000 h was FCS N°4, FCS N°3, FCS N°2, and FCS N°1. As can be seen from Fig. 8, the FCSs were actually used in this order from 2000 h to 3000 h.

From 3000 h to 4000 h, the final operating order of FCSs was FCS N°1, FCS N°4, FCS N°2, FCS N°3, as the first scheduling in descending order of RULs at $t = 3,000\,h$ was FCS N°3, FCS N°4, FCS N°2, FCS N°1. The first position occupied by the FCS N°4 from 2000 h to 3000 h enabled it to slow down its aging process, indeed (Fig. 10). This degradation trend improvement was learned by the RUL prognostic model as well, because at $t = 3,000\,h$, the FCS N°4 was no longer the last FCS in the queue but the second one (Fig. 9). However, due to the small amount of training data available at that time, the significant slope variation observed from $t = 2,000\,h$ in the degradation trend could not be captured accurately by the prognostic model. As a result, FCS N°3's RUL was higher than that of FCS N°4 at $t = 3,000\,h$. Actually, the FCS N°4 should have the best RUL at that moment. This error was rectified by the prognostic algorithm at the next prediction session (at $t = 4,000\,h$), as new maximum power samples were added to the time series between $t = 3,000\,h$ and $t = 4,000\,h$. It is worth noting the consistency between FCSs' scheduling in descending order of RULs at $t = 4,000\,h$, which is FCS N°1, FCS N°4, FCS N°2, FCS N°3 (Fig. 9) and their scheduling in ascending order of cycling degradation at $t = 4,000\,h$ (Fig. 10). The final operating order of FCSs from 4000 h to 5000 h was exactly the expected final scheduling (FCS N°3, FCS N°4, FCS N°2, and FCS N°1).

FCSs' operating order was continuously updated every 5 h, first in descending order of RULs and then regarding their previous operating mode. After each final scheduling update, the power $P_{required_{MFCS}}$ required from the MFCS system was distributed between FCSs according to the advanced Daisy-Chain principle applied in this paper, until the MFCS system reached its EoL at $t = 12,422\,h$, as shown in Fig. 8. It should be noted that, the MFCS system is considered at its EoL as soon as the battery is discharged while the MFCS system is operating in degraded mode. Indeed, when operating in degraded mode, the MFCS system is undersized and cannot meet the requirements for a proper battery use, healthily speaking. In Fig. 8, the degraded mode operation of the MFCS system started at $t = 12,200\,h$ when the FCS N°1 reached its EoL (loss of 10% of the maximum power) and the battery got discharged at $t = 12,422\,h$. Additionally, 982.4 kg of H_2 were consumed over the lifetime of the MFCS system to meet the load demand.

The hybrid MFCS/battery system's energy management is also

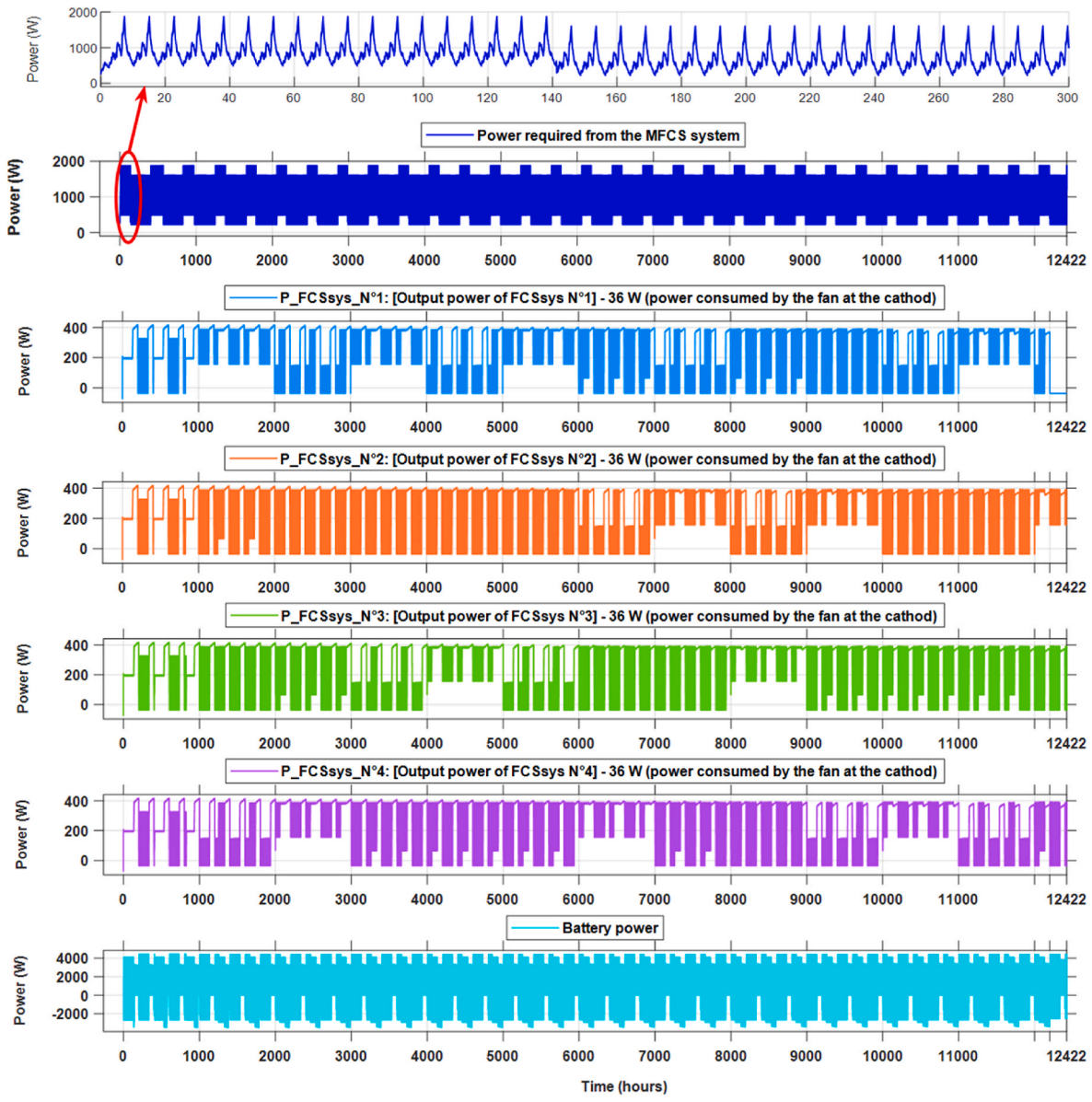

Fig. 8. Distribution of the power required from the MFCS system between the four FCS systems; battery power [RUL prognostic-based adaptive Daisy-Chain EMS].

carried out by the equidistributional and the Daisy-Chain EMSs to highlight the performance of the proposed EMS. For the comparative study to be fair, these conventional EMSs are revised to operate FCSs only in their safe power range, as the proposed EMS did.

5.3. Hybrid MFCS/battery system simulation results under conventional EMSs

When applying the equidistributional EMS and the Daisy-Chain EMS to the MFCS system over the entire simulation time, the system reaches its EoL after only 5000 h, and 5214 h, respectively. In addition to the non-adaptive nature of these conventional EMSs, three reasons can explain the lifetime improvement observed with the proposed EMS.

- Firstly, the proposed EMS is based on the Daisy-Chain principle. By allocating $P_{required_{MFCS}}$ to the first FCS in the queue, one of the FCSs in the MFCS system usually experienced very few start-stop cycles.
- Secondly, the proposed EMS updates FCSs operating order to balance their degradation levels. This offers to each FCS the advantage of being the first FCS in the queue, which results in a reduced frequency of start-stop cycles.
- Finally, when the remaining power demand has to be supplied by a FCS, but it is out of the FCS safe power range, the proposed EMS optimizes the start-stop cycles of this FCS by checking it current state (on or off) before deciding whether to operate it or shut it down.

In conclusion, operating the MFCS system under the equidistributional and the Daisy-Chain strategies instead of the proposed EMS, results respectively in a loss of 59.75% and 58.03% on the MFCS system's lifetime. However, the equidistributional strategy would make the hybrid MFCS/battery system consume less hydrogen than the proposed strategy for the same operating time. For 5000 operating hours, the hybrid system consumed approximately 389.2 kg of hydrogen under the proposed EMS versus 356.2 kg under the equidistributional strategy, representing a reduction in hydrogen consumption of around 8.48%. Indeed, the equitable distribution of power demand between FCSs resulted in FCSs operating mostly in the low current density zone, which is very close to the best energy efficiency zone for FCSs. On the other hand, under the proposed EMS and the Daisy-Chain EMS, FCSs were

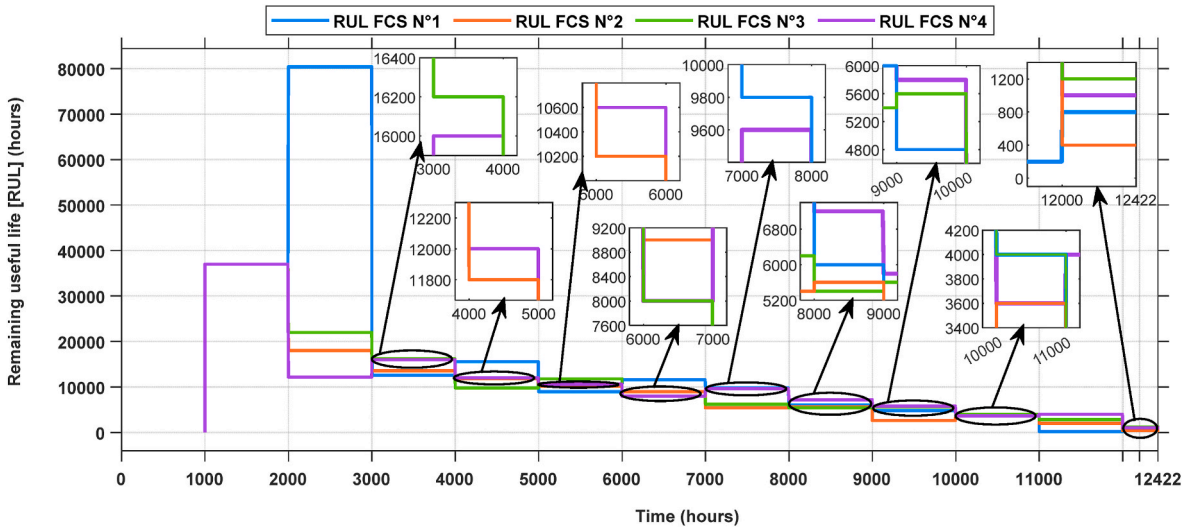

Fig. 9. FCSs' RUL prognostic every 5 h [RUL prognostic-based adaptive Daisy-Chain EMS].

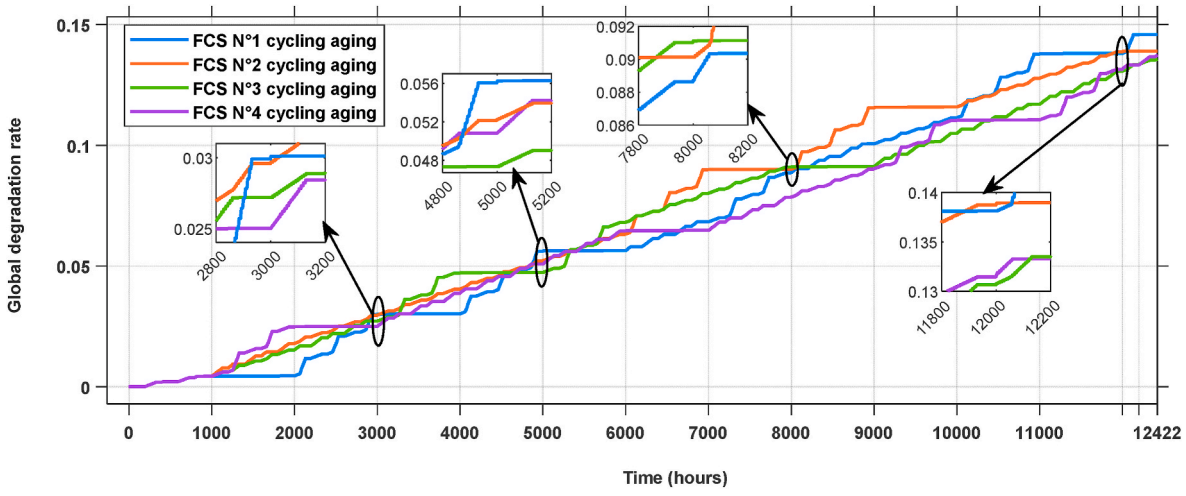

Fig. 10. FCSs' cycling aging evolution [RUL prognostic-based adaptive Daisy-Chain EMS].

mostly operated in the high current density range to meet the power demand using the minimum number of FCSs.

Tables 1–2 summarize respectively the comparative analysis of the MFCS system's lifetime and hydrogen consumption under the proposed EMS vs. the conventional EMSs.

Before concluding this work, the proposed EMS should be compared with the reference EMS, which is the SOH estimation-based adaptive Daisy-Chain EMS, to check whether the potential errors in the RUL prediction affects the ultimate lifetime of the MFCS system or not.

6. reference EMS simulation results

The SOH estimation-based adaptive Daisy-Chain EMS is a variant of the proposed EMS, as FCSs' operating order would be updated based on their SOH estimations instead of their RULs. This strategy can be seen as the reference EMS regarding the energy management principle applied in this paper, since SOH estimations would be definitely more accurate than RUL predictions. The prognostic algorithm may not be able to capture significant changes in FCSs' degradation trends accurately. Although the resulting RUL predictions errors can be corrected as the

Table 1
MFCS system's lifetime under the RUL prognostic-based adaptive Daisy-Chain EMS vs. conventional EMSs.

EMS	Proposed EMS	Equidistributional EMS	Daisy-Chain EMS
MFCS system's lifetime	12,422 h	5000 h	5214 h
Gain	–	2.48	2.38

Table 2
MFCS system's H_2 consumption under the RUL prognostic-based adaptive Daisy-Chain EMS vs. conventional EMSs.

EMS	Proposed EMS		Equidistributional EMS	Daisy-Chain EMS
MFCS system's H_2 consumption	t = 5000 h t = 5214 h t = 12,422 h	389.2 kg 405 kg 982.4 kg	356.2 kg	404.4 kg
H_2 consumption reducing compared to the proposed EMS	–		8.48 %	0.15 %

amount of training data increases, it could be hard to know if the post-prognostic decisions adjustments were enough to extend the MFCS system's lifetime as much as it would be when using more accurate information like FCSs' SOH estimations. To investigate this, the hybrid MFCS/battery system simulation results under the reference EMS are presented in this section.

In the reference EMS, FCSs' maximum powers are resampled each 5 h so their operating order will be updated at the same frequency as in the RUL prognostic-based adaptive Daisy-Chain EMS (proposed EMS). Under the reference EMS, the MFCS system reached its EoL in 12,460 h, which is just 38 h longer than the lifetime obtained under the proposed EMS. Therefore, it is quite acceptable to conclude that the proposed strategy extends the MFCS system's lifetime as much as the reference EMS, although RUL prognostics are not as accurate as maximum power estimations.

Furthermore, the hydrogen consumption of the hybrid system under the reference strategy from $t = 0\,h$ to $t = 12,422\,h$ would be around 984.6 kg (i.e., 2.2 kg more than the amount of hydrogen consumed under the proposed EMS).

It can be concluded from these results that the comparative study of the RUL prognostic-based energy management concept for MFCS systems and the SOH estimation-based energy management approach deserves further investigation. Using FCSs' RUL prognostics in MFCS systems energy management could simplify adaptive EMSs design compared to the SOH estimation-based energy management approach. In fact, the SOH of a FCS can only decrease over time, whereas its RUL can actually increase between two consecutive prognostic sessions. This makes the RUL a suitable parameter to analyze when making adaptive energy management decisions.

7. Conclusion

A health-conscious EMS is proposed for MFCS systems in this paper to improve their lifetime. This study is part of the PHM framework, which has seen significant progress over the last decade in FCSs RUL prognostic algorithm development for appropriate energy management decision-making regarding FCSs' durability. Therefore, an ANN-based prognostic algorithm was proposed for FCSs real-world use in automotive applications and combined with an advanced Daisy-Chain energy management principle to investigate the prognostic-based energy management concept under a real vehicle use scenario.

The proposed strategy was referred to as RUL prognostic-based adaptive Daisy-Chain EMS. By integrating RUL prognostics into the Daisy-Chain energy management principle, it was possible to balance FCSs' degradation levels, thus preventing the MFCS system from too early degraded mode operation. Indeed, operating in degraded mode signifies that the MFCS system is reaching its EoL, as it will eventually be unable to meet the load requirements.

The RUL prognostic-based adaptive Daisy-Chain EMS has been validated through simulations in Matlab/Simulink environment. The simulations were performed on an MFCS system consisting of four 500 W-Horizon FCSs using the WLTP class 3 driving cycle.

A comparative analysis of the MFCS system performance was conducted under the proposed EMS and two conventional EMSs (The equidistributional and the Daisy-Chain EMSs). The results showed that the proposed EMS can extend the MFCS system's lifetime by over 2.48 and 2.38 times compared to the equidistributional and the Daisy-Chain EMSs, respectively.

In terms of hydrogen consumption, the MFCS system consumed almost the same amount of hydrogen under both the proposed EMS and the Daisy-Chain strategy. However, approximately 8.48% of hydrogen was saved under the equidistributional EMS, as FCSs were often operated in their best energy-efficient regions (low current density range) due to the equitable distribution of power demand between them. It should be reminded that under the proposed EMS and the Daisy-Chain EMS, FCSs were mostly operated in their high current density range to meet the power demand using the minimum number of FCSs.

A last comparison study was conducted in this paper between the proposed EMS and the reference EMS which is based on FCSs' SOH estimations. The proposed strategy has been found as reliable as the reference strategy although RUL prognostics may not be as accurate as SOH estimations.

This work can be considered as a proof of concept. The next future research objective in this area is to focus on integrating FCSs' RUL prognostics into MFCS systems energy management through an optimization approach.

CRediT authorship contribution statement

W. René Bankati: Writing – review & editing, Writing – original draft, Conceptualization. **Loïc Boulon:** Supervision, Resources, Funding acquisition. **Samir Jemei:** Supervision, Resources, Funding acquisition.

Declaration of competing interest

The authors declare that they have no known competing financial interests or personal relationships that could have appeared to influence the work reported in this paper.

Acknowledgments

This work has been supported by the Universalis Causa program of UQTR in Canada, the EIPHI Graduate School (contract ANR-17-EURE-0002) and the Region Bourgogne Franche-Comté in France.

References

[1] Pramuanjaroenkij A, Kakaç S. The fuel cell electric vehicles: the highlight review. Int J Hydrogen Energy 2023;48(25):9401–25. https://doi.org/10.1016/j.ijhydene.2022.11.103.
[2] Agyekum EB, Odoi-Yorke F, Abbey AA, Ayetor GK. A review of the trends, evolution, and future research prospects of hydrogen fuel cells – a focus on vehicles. Int J Hydrogen Energy 2024;72:918–39. https://doi.org/10.1016/j.ijhydene.2024.05.480.
[3] Ahmad S, Nawaz T, Ali A, Orhan MF, Samreen A, Kannan AM. An overview of proton exchange membranes for fuel cells: materials and manufacturing. Int J Hydrogen Energy 2022;47(44):19086–131. https://doi.org/10.1016/j.ijhydene.2022.04.099.
[4] Shu Q, Yang S, Zhang X, Li Z, Zhang Y, Tang Y, Gao H, Xia C, Zhao M, Li X, Zhao H. A systematic investigation on the effects of Cu2+ contamination on the performances and durability of proton exchange membrane fuel cells. Int J Hydrogen Energy 2024;57:90–9. https://doi.org/10.1016/j.ijhydene.2024.01.011.
[5] Whiston MM, Azevedo IL, Litster S, Whitefoot KS, Samaras C, Whitacre JF. Expert assessments of the cost and expected future performance of proton exchange membrane fuel cells for vehicles. Proc Natl Acad Sci U S A 2019 Mar 12;116(11):4899–904. https://doi.org/10.1073/pnas.1804221116.
[6] Yue M, Al Masry Z, Jemei S, Zerhouni N. An online prognostics-based health management strategy for fuel cell hybrid electric vehicles. Int J Hydrogen Energy 2021;46(24):13206–18. https://doi.org/10.1016/j.ijhydene.2021.01.095.
[7] de-Troya JJ, Álvarez C, Fernández-Garrido C, Carral L. Analysing the possibilities of using fuel cells in ships. Int J Hydrogen Energy 2016;41(4):2853–66. https://doi.org/10.1016/j.ijhydene.2015.11.145.
[8] Kallo J. DLR leads HY4 project for four-seater fuel cell aircraft. Fuel Cell Bull 2015;2015(11):13. https://doi.org/10.1016/S1464-2859(15)30362-X.
[9] Shi W, Huangfu Y, Xu L, Pang S. Online energy management strategy considering fuel cell fault for multi-stack fuel cell hybrid vehicle based on multi-agent reinforcement learning. Appl Energy 2022;328:120234. https://doi.org/10.1016/j.apenergy.2022.120234.
[10] Qiu Y, Zeng T, Zhang C, Wang G, Wang Y, Hu Z, Yan M, Wei Z. Progress and challenges in multi-stack fuel cell system for high power applications: architecture and energy management. Green Energy and Intelligent Transportation 2023;2(2):100068. https://doi.org/10.1016/j.geits.2023.100068.
[11] Marx N, Boulon L, Gustin F, Hissel D, Agbossou K. A review of multi-stack and modular fuel cell systems: interests, application areas and on-going research activities. Int J Hydrogen Energy 2014;39(23):12101–11. https://doi.org/10.1016/j.ijhydene.2014.05.187.
[12] Liang Y, Liang Q, Zhao J, He J. Downgrade power allocation for multi-fuel cell system (MFCS) based on minimum hydrogen consumption. Energy Rep 2022;8:15574–83. https://doi.org/10.1016/j.egyr.2022.11.126.
[13] Macias Fernandez A, Kandidayeni M, Boulon L, Chaoui H. An adaptive state machine based energy management strategy for a multi-stack fuel cell hybrid electric vehicle. IEEE Trans Veh Technol Jan. 2020;69(1):220–34. https://doi.org/10.1109/TVT.2019.2950558.

[14] Marx N, Hissel D, Gustin F, Boulon L, Agbossou K. On the sizing and energy management of an hybrid multistack fuel cell – battery system for automotive applications. Int J Hydrogen Energy 2017;42(2):1518–26. https://doi.org/10.1016/j.ijhydene.2016.06.111.
[15] Jian B, Wang H. Hardware-in-the-loop real-time validation of fuel cell electric vehicle power system based on multi-stack fuel cell construction. J Clean Prod 2022;331:129807. https://doi.org/10.1016/j.jclepro.2021.129807.
[16] Zhang G, Zhou S, Gao J, Fan L, Lu Y. Stacks multi-objective allocation optimization for multi-stack fuel cell systems. Appl Energy 2023;331:120370. https://doi.org/10.1016/j.apenergy.2022.120370.
[17] Moghadari M, Kandidayeni M, Boulon L, Chaoui H. Operating cost comparison of a single-stack and a multi-stack hybrid fuel cell vehicle through an online hierarchical strategy. IEEE Trans Veh Technol Jan. 2023;72(1):267–79. https://doi.org/10.1109/TVT.2022.3205879.
[18] Han X, Li F, Zhang T, Zhang T, Song K. Economic energy management strategy design and simulation for a dual-stack fuel cell electric vehicle. Int J Hydrogen Energy 2017;42(16):11584–95. https://doi.org/10.1016/j.ijhydene.2017.01.085.
[19] Wang T, Li Q, Yin L, Chen W. Hydrogen consumption minimization method based on the online identification for multi-stack PEMFCs system. Int J Hydrogen Energy 2019;44(11):5074–81. https://doi.org/10.1016/j.ijhydene.2018.09.181.
[20] Wang Y, Chen W, Li Q, Han Y, Guo A, Wang T. Coordinated optimal power distribution strategy based on maximum efficiency range of multi-stack fuel cell system for high altitude. Int J Hydrogen Energy 2024;50(Part C):374–87. https://doi.org/10.1016/j.ijhydene.2023.08.177.
[21] Ghaderi R, Kandidayeni M, Boulon L, Trovão JP. Quadratic programming based energy management in a multi-stack fuel cell hybrid electric vehicle. In: 2021 IEEE vehicle power and propulsion conference (VPPC); 2021. p. 1–6. https://doi.org/10.1109/VPPC53923.2021.9699348. Gijon, Spain.
[22] Zhou S, Zhang G, Fan L, Gao J, Pei F. Scenario-oriented stacks allocation optimization for multi-stack fuel cell systems. Appl Energy 2022;308:118328. https://doi.org/10.1016/j.apenergy.2021.118328.
[23] Zheng W, Lv B, Shao Z, Zhang B, Liu Z, Sun J, Yuan J, Jiang C. Optimization of power allocation for the multi-stack PEMEC system considering energy efficiency and degradation. Int J Hydrogen Energy 2024;53:1210–25. https://doi.org/10.1016/j.ijhydene.2023.11.241.
[24] Li Q, Cai L, Yin L, Wang T, Li L, Xie S, Chen W. An energy management strategy considering the economy and lifetime of multistack fuel cell hybrid system. IEEE Transactions on Transportation Electrification June 2023;9(2):3498–507. https://doi.org/10.1109/TTE.2022.3218505.
[25] Khalatbarisoltani A, Kandidayeni M, Boulon L, Hu X. Comparison of decentralized ADMM optimization algorithms for power allocation in modular fuel cell vehicles. IEEE ASME Trans Mechatron Oct. 2022;27(5):3297–308. https://doi.org/10.1109/TMECH.2021.3105950.
[26] Xie P, Asgharian H, Guerrero JM, Vasquez JC, Araya SS, Liso V. A two-layer energy management system for a hybrid electrical passenger ship with multi-PEM fuel cell stack. Int J Hydrogen Energy 2024;50(Part B):1005–19. https://doi.org/10.1016/j.ijhydene.2023.09.297.
[27] Wang L, Li X, Guo P, Guo S, Yang Z, Pei P. Bibliometric analysis of prognostics and health management (PHM) in hydrogen fuel cell engines. Int J Hydrogen Energy 2022;47(80):34216–43. https://doi.org/10.1016/j.ijhydene.2022.08.024.
[28] Zuo J, Steiner NY, Li Z, Hissel D. Health management review for fuel cells: focus on action phase. Renew Sustain Energy Rev 2024;201:114613. https://doi.org/10.1016/j.rser.2024.114613.
[29] Bahrami M, Martin J, Maranzana G, Pierfederici S, Weber M, Didierjean S. Fuel cell management system: an approach to increase its durability. Appl Energy 2022;306 (Part B):118070. https://doi.org/10.1016/j.apenergy.2021.118070.
[30] Xu L, Li J, Ouyang M, Hua J, Li X. Active fault tolerance control system of fuel cell hybrid city bus. Int J Hydrogen Energy 2010;35(22):12510–20. https://doi.org/10.1016/j.ijhydene.2010.08.005.
[31] Dijoux E, Steiner NY, Benne M, Péra M, Grondin-Perez B. Experimental validation of an active fault tolerant control strategy applied to a proton exchange membrane fuel cell. Electrochemistry (Tokyo, Jpn) 2022;3:633–52. https://doi.org/10.3390/electrochem3040042.
[32] Yan C, Chen J, Liu H, Kumar L, Lu H. Health management for PEM fuel cells based on an active fault tolerant control strategy. IEEE Trans Sustain Energy April 2021; 12(2):1311–20. https://doi.org/10.1109/TSTE.2020.3042990.
[33] Wang P, Liu H, Chen J, Qin X, Lehnert W, Shao Z, Li R. A novel degradation model of proton exchange membrane fuel cells for state of health estimation and prognostics. Int J Hydrogen Energy 2021;46(61):31353–61. https://doi.org/10.1016/j.ijhydene.2021.07.004.
[34] Jouin M, Gouriveau R, Hissel D, Péra M, Zerhouni N. Prognostics of PEM fuel cell in a particle filtering framework. Int J Hydrogen Energy 2014;39(1):481–94. https://doi.org/10.1016/j.ijhydene.2013.10.054.
[35] Chen K, Laghrouche S, Djerdir A. Aging prognosis model of proton exchange membrane fuel cell in different operating conditions. Int J Hydrogen Energy 2020; 45(20):11761–72. https://doi.org/10.1016/j.ijhydene.2020.02.085.
[36] Tang X, Qin X, Wei K, Xu S. A novel online degradation model for proton exchange membrane fuel cell based on online transfer learning. Int J Hydrogen Energy 2023; 48(36):13617–32. https://doi.org/10.1016/j.ijhydene.2022.12.260.
[37] Zhang S, Chen T, Xiao F, Zhang R. Degradation prediction model of PEMFC based on multi-reservoir echo state network with mini reservoir. Int J Hydrogen Energy 2022;47(94):40026–40. https://doi.org/10.1016/j.ijhydene.2022.09.160.
[38] Jin J, Chen Y, Xie C, Wu F. Remaining useful life prediction of PEMFC based on the multi-input cycle reservoir with jump network. Int J Hydrogen Energy 2023;48 (34):12844–60. https://doi.org/10.1016/j.ijhydene.2022.12.170.
[39] Benaggoune K, Yue M, Jemei S, Zerhouni N. A data-driven method for multi-step-ahead prediction and long-term prognostics of proton exchange membrane fuel cell. Appl Energy 2022;313:118835. https://doi.org/10.1016/j.apenergy.2022.118835.
[40] Zhai Y, Yin C, Wang R, Liu M, Hou Y, Tang H. Degradation prediction of 65 kW proton exchange membrane fuel cells on city buses using a hybrid approach with the advantage actor-critic method. Int J Hydrogen Energy 2024;50(Part C):414–27. https://doi.org/10.1016/j.ijhydene.2023.08.191.
[41] Xie R, Ma R, Pu S, Xu L, Zhao D, Huangfu Y. Prognostic for fuel cell based on particle filter and recurrent neural network fusion structure. Energy and AI 2020;2: 100017. https://doi.org/10.1016/j.egyai.2020.100017.
[42] Jemei S. Hybridization, diagnostic and prognostic of proton exchange membrane fuel cells. London: ISTE Ltd; 2018.
[43] Yue M, Jemei S, Zerhouni N. Health-conscious energy management for fuel cell hybrid electric vehicles based on prognostics-enabled decision-making. IEEE Trans Veh Technol Dec. 2019;68(12):11483–91. https://doi.org/10.1109/TVT.2019.2937130.
[44] Zuo J, Cadet C, Li Z, Berenguer C, Outbib R. Post-prognostics decision-making strategy for load allocation on a stochastically deteriorating multi-stack fuel cell system. Proc Inst Mech Eng O J Risk Reliab 2023;237(1):40–57. https://doi.org/10.1177/1748006X221086381.
[45] Herr N, Nicod J, Varnier C, Jardin L, Sorrentino A, Hissel D, Péra M. Decision process to manage useful life of multi-stacks fuel cell systems under service constraint. Renew Energy 2017;105:590–600. https://doi.org/10.1016/j.renene.2017.01.001.
[46] Zuo J, Cadet C, Li Z, Bérenguer C, Outbib R. Post-prognostics decision making strategy to manage the economic lifetime of a two-stack PEMFC system. 2021 annual reliability and maintainability symposium (RAMS). 2021. p. 1–7. https://doi.org/10.1109/RAMS48097.2021.9605719. Orlando, FL, USA.
[47] Dirkes S, Leidig J, Fisch P, Pischinger S. Prescriptive Lifetime Management for PEM fuel cell systems in transportation applications, Part I: state of the art and conceptual design. Energy Convers Manag 2023;277:116598. https://doi.org/10.1016/j.enconman.2022.116598.
[48] Truong HVA, Dao HV, Do TC, Ho CM, To XD, Dang TD, Ahn KK. Mapping fuzzy energy management strategy for PEM fuel cell–battery–supercapacitor hybrid excavator. Energies 2020;13:3387. https://doi.org/10.3390/en13133387.
[49] Wallnöfer-Ogris E, Poimer F, Köll R, Macherhammer M, Trattner A. Main degradation mechanisms of polymer electrolyte membrane fuel cell stacks – mechanisms, influencing factors, consequences, and mitigation strategies. Int J Hydrogen Energy 2024;50:1159–82. https://doi.org/10.1016/j.ijhydene.2023.06.215. Part B.
[50] Dépature C, Macías A, Jácome A, Boulon L, Solano J, Trovão JP. IEEE VTS motor vehicles challenge 2017 - energy management of a fuel cell/battery vehicle. In: 2016 IEEE vehicle power and propulsion conference (VPPC); 2016. p. 1–6. https://doi.org/10.1109/VPPC.2016.7791701. Hangzhou, China.
[51] Kandidayeni M, Macias A, Boulon L, Kelouwani S. Investigating the impact of ageing and thermal management of a fuel cell system on energy management strategies. Appl Energy 2020;274:115293. https://doi.org/10.1016/j.apenergy.2020.115293.
[52] Ettihir K, Boulon L, Agbossou K. Energy management strategy for a fuel cell hybrid vehicle based on maximum efficiency and maximum power identification. IET Electr Syst Transp 2016;6:261–8. https://doi.org/10.1049/iet-est.2015.0023.
[53] Legala A, Shahgaldi S, Li X. Data-based modelling of proton exchange membrane fuel cell performance and degradation dynamics. Energy Convers Manag 2023;296: 117668. https://doi.org/10.1016/j.enconman.2023.117668.
[54] Dépature C, Macías A, Jácome A, Boulon L, Solano J, Trovão JP. Fuel cell/supercapacitor passive configuration sizing approach for vehicular applications. Int J Hydrogen Energy 2020;45(50):26501–12. https://doi.org/10.1016/j.ijhydene.2020.05.040.
[55] Zhou J, Liu J, Xue Y, Liao Y. Total travel costs minimization strategy of a dual-stack fuel cell logistics truck enhanced with artificial potential field and deep reinforcement learning. Energy 2022;239(Part A):121866. https://doi.org/10.1016/j.energy.2021.121866.